

Article

# Gasification Characteristics and Kinetics of Unburned Pulverized Coal in Blast Furnaces

Rian Zan <sup>1</sup>, Wei Wang <sup>1,\*</sup>, Runsheng Xu <sup>1,\*</sup>, Johannes Schenk <sup>2</sup> , Heng Zheng <sup>2</sup> and Haoxiang Wang <sup>1</sup>

<sup>1</sup> State Key Laboratory of Refractories and Metallurgy, Key Laboratory for Ferrous Metallurgy and Resources Utilization of Ministry of Education, Wuhan University of Science and Technology, Wuhan 430081, China; ZanRian163@163.com (R.Z.); wanghaoxiang\_123@163.com (H.W.)

<sup>2</sup> Chair of Ferrous Metallurgy, Montanuniversität Leoben, Franz-Josef-Straße 18, A-8700 Leoben, Austria; Johannes.Schenk@unileoben.ac.at (J.S.); zhengheng6728@163.com (H.Z.)

\* Correspondence: wangwei74@wust.edu.cn (W.W.); xu\_runsheng@163.com (R.X.); Tel.: +86-139-7143-6542 (W.W.); +86-188-1049-0945 (R.X.)

Received: 21 September 2019; Accepted: 9 November 2019; Published: 13 November 2019



**Abstract:** Pulverized coal injected into a blast furnace (BF) burns incompletely in a very limited amount of time. A considerable amount of unburned pulverized coal (UPC) escapes from the raceway to the coke layer. The unburned pulverized coal reacts with CO<sub>2</sub> in the coke layer, and this has a very significant impact on the operation of the BF. The gasification reaction characteristics of the UPC with CO<sub>2</sub> were assessed by thermogravimetric analysis. The microstructure and specific surface area of the pulverized coal and UPC were characterized by scanning electron microscopy (SEM), and a specific surface area testing apparatus together with the Brunauer-Emmett-Teller (BET) method, respectively. The results showed that Qingding UPC requires a higher temperature to complete the gasification reaction. At the same heating rate, the  $T_m$  (maximum reaction rate temperature) of the Shenhua UPC is much lower and the reaction rate is larger than those of the Qingding UPC. An increased heating rate is beneficial for the gasification reaction of the two UPCs. The kinetics analysis results showed that the optimal mechanism function models for the Shenhua and Qingding UPCs are chemical reaction models. The apparent activation energies of gasification of the Shenhua UPC and Qingding UPC under different conditions were 269.89–223.41 KJ/mol and 266.70–251.54 KJ/mol, respectively.

**Keywords:** unburned pulverized coal; gasification; kinetic characteristics

## 1. Introduction

Presently, global warming and air pollution are becoming extremely serious concerns and are attracting increasing attention. Notably, the iron and steel industry need to prioritize reducing CO<sub>2</sub> emissions. The amount of CO<sub>2</sub> emissions from iron and steel plants accounts for 5–7% of the total global CO<sub>2</sub> emissions [1,2]. To reduce the cost of ironmaking and the emissions of CO<sub>2</sub> and other polluting gases, iron and steel enterprises worldwide have carried out studies on reducing the coke ratio. Many new technologies to reduce the use of coke in blast furnaces (BFs), such as pulverized coal injection (PCI), ferro-coke technology and natural gas injection have been adopted [3–7]. PCI is a useful method that can reduce coke consumption and ironmaking costs. Coal injection with high oxygen enrichment has become a mainstream BF approach [8,9].

Mathieson et al. [10] noted that the combustion of pulverized coal is always incomplete in a limited time. A large amount of unburned pulverized coal (UPC) escapes from the raceway and enters the coke bed. A schematic of UPC production and the movement track is shown in Figure 1. Xiang et al. [11] also stated that a large amount of UPC is present in the blast furnace because the pulverized coal

cannot be completely burned in a space with a narrow tuyere. Generally, a large amount of coal is injected to minimize the coke ratio in the BF. Once the amount of coal injection has increased to a certain extent, a large amount of UPC appears in the BF [12]. The UPC behaves in several ways: it participates in the gasification reaction of carbon; it participates in the carburization reaction of the hot metal; it participates in the direct reduction reaction of iron; it deposits in the slag; and it escapes with the gas [13]. When the amount of UPC reaches a certain threshold, it adversely affects the BF operation, for example, by creating poor permeability and unstable pressure [14]. Yu et al. [15] studied the behavior of UPC using a thermal model of a coke-packed bed under similar operational conditions as those at Baosteel. The results showed that UPC participates in the gasification reaction of coke at 1100 °C, and the strength of the coke increases from 55.9% to 63.2%. The existence of an appropriate amount of UPC can protect coke from degradation. Takashi [16] used a mathematical model to quantitatively analyze the movement and accumulation of UPC in the lower part of the BF. The results indicated that the movement of UPC was affected by the gas flow rate, particle size and amount of pulverized coal. Diao et al. [17] analyzed the effect of UPC on the slag viscosity by adding UPC to the slag. The results indicated that the slag viscosity increased with the addition of UPC. Iwanaga [18] studied the effects of different proportion of CO<sub>2</sub>, CO, N<sub>2</sub> and different temperature on the gasification reaction of unburned coal and coke. The results showed that the gasification reaction rate of unburned coal was seven times that of coke, and unburned coal inhibited the degradation of coke.

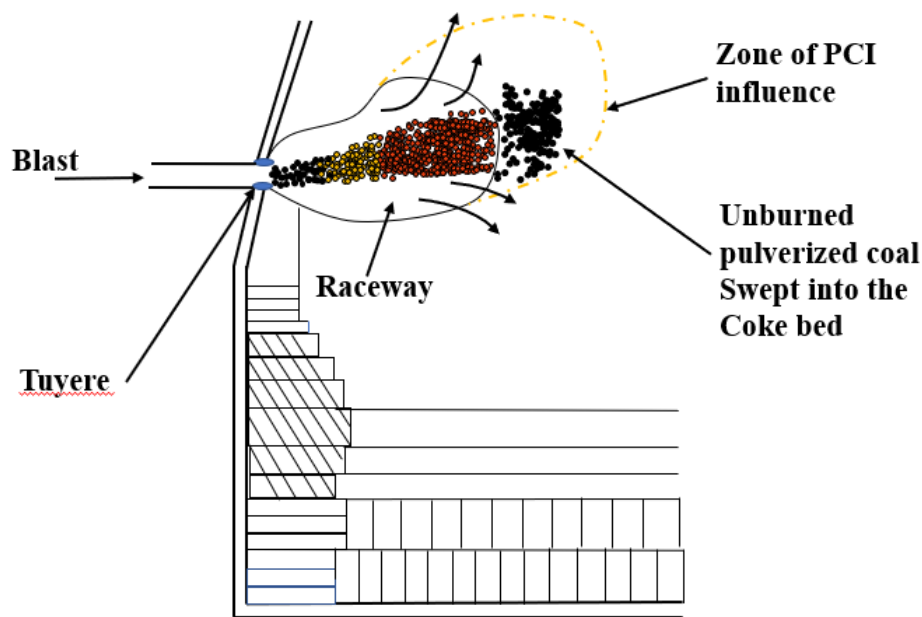


**Figure 1.** Production of unburned pulverized coal (UPC) and movement behavior in a blast furnace (BF).

Xiang et al. [11] investigated the combustion characteristics of two kinds of UPC by using the thermogravimetric analysis method and the reaction kinetics mechanism of UPC gasification with CO<sub>2</sub> at 1000–1100 °C. An excellent kinetic analysis was conducted and it has greatly enhanced the understanding of the reaction kinetics of coal in a blast furnace. However, the UPC was prepared in a high-temperature furnace in Xiang's study; this equipment was not able to simulate the injection status of coal with high speed in the raceway.

In order to simulate the conditions of a blast furnace raceway more realistically, self-developed equipment was used in this study. The UPC was prepared with a high temperature and a high speed in the simulated blast furnace atmosphere. Furthermore, the gasification characteristics of two typical kinds of UPCs at different heating rates were studied in this paper. The kinetic parameters of the gasification reaction were calculated by the gas-solid reaction mechanism function. The microstructure and specific surface area of the pulverized coal and UPC were characterized by scanning electron

microscopy (SEM) and a specific surface area testing apparatus along with the Brunauer-Emmett-Teller (BET) method to reveal the gasification behavior of UPC powder in a BF. This study helps in the selection of pulverized coal and provides a theoretical basis for the improvement of coal injection operations.

## 2. Experimental Materials and Methods

### 2.1. Raw Materials

The two kinds of pulverized coal (Shenhua and Qingding) used in this study were from a BF in China. After screening, pulverized coal with a particle size of 160–200 mesh was selected as the experimental material. The proximate and ultimate analyses of the Shenhua and Qingding pulverized coal was carried out according to the Chinese standard (GB/T212-2008 and GB/T214-2007, GB/T476-2008). The results are shown in Table 1. From the proximate analysis, the fixed carbon and ash content of the Qingding pulverized coal is much higher than that of Shenhua pulverized coal, but the moisture and volatile matter content are much lower.

**Table 1.** Proximate and ultimate analysis of Shenhua and Qingding pulverized coal (mass %), air dry basis.

Sample	Proximate Analysis				Ultimate Analysis				
	Moisture	Volatiles	Ash	Fixed Carbon	C	H	O	N	St
Shenhua	5.27	23.94	4.98	65.81	68.31	4.89	10.23	0.86	0.26
Qingding	1.20	7.99	12.25	78.56	83.57	0.17	1.99	0.97	0.71

### 2.2. Experimental Equipment and Methods

#### 2.2.1. Combustion Conversion Degree

The Shenhua UPC and Qingding UPC were prepared using a self-developed coal injection simulation device. This device consisted of a hot blast stove, coal combustion furnace, coal injection lance, and a data acquisition and control system. The hot blast furnace and coal combustion furnace were heated using a MoSi<sub>2</sub> heating element. The height and inner diameter of the alumina tube in the hot blast stove are 560 mm and 60 mm, respectively, and the height and inner diameter of the alumina tube in the combustion furnace are 1050 mm and 55 mm, respectively. Because the actual blast temperature of the BF was 1100–1250 °C [17], the air flow needed to be heated from ambient temperature to 1200 °C through the hot blast stove. In order to achieve this target, the temperature of the hot blast stove was set as 1400 °C, and the temperature of the pulverized coal combustion furnace was set as 1200 °C. The coal injection lance is shown as 14 in Figure 2, and it is composed of an upper pulverized coal bunker (capacity: 10 g), a pulverized coal conveying winch, rotating motor and coal injection pipe. The pulverized coal in the coal bunker was transported into the coal injection pipe for injection through the winch driven by the motor. When the certain amount of pulverized coal was transported, the N<sub>2</sub> injection valve was opened, and the pulverized coal was fed into the combustion furnace by a N<sub>2</sub> gas jet for the combustion reaction. The heating temperature was controlled by the PID(proportional-integral-derivative control)-controllers, and the gas flow was controlled by the mass flowmeter. The device control software was developed by the Xingyuanda Company and installed in a computer to obtain the experimental data and adjust the operation parameters.

The UPC was prepared as follows. First, we prepared 50 g pulverized coal samples of less than 200 meshes, weighed 10 g of the pulverized coal samples and put them into the coal bunker. Secondly, we heated the hot blast stove and combustion furnace. The pulverized coal combustion furnace was heated to 950 °C in 100 min, then increased from 950 °C to 1200 °C in 60 min, and then kept at 1200 °C. The hot blast stove was heated to 200 °C in 30 min, increased from 200 °C to 800 °C in 60 min, then increased from 800 °C to 1400 °C in 100 min, and then held at 1400 °C. Thirdly, the air was blown into the hot blast stove at a flow rate of 20 L/min. The air passed through the hot blast stove and then

arrived at the pulverized coal combustion stove to participate in the coal combustion. Fourthly, after the hot blast stove and the pulverized coal combustion furnace were raised to the specified temperature and stabilized for 5 min, and then the coal injection operation started. N<sub>2</sub> was used as the carrier gas, and the rotating frequency of the stepping rotating motor was 50 R/min. After 1 min rotating, the N<sub>2</sub> valve was opened, and the coal in the injection pipe was blown into the combustion furnace. In this experiment, the coal injection rate was about 0.371 g/min, and the interval between two injections was 5 s. Finally, after the experiment was completed, the ash collecting tank was removed and the UPC was collected. The experimental simulation device for BF coal injection is shown in Figure 2. After screening the UPC, particles of 160–200 mesh were selected for the subsequent experiments.

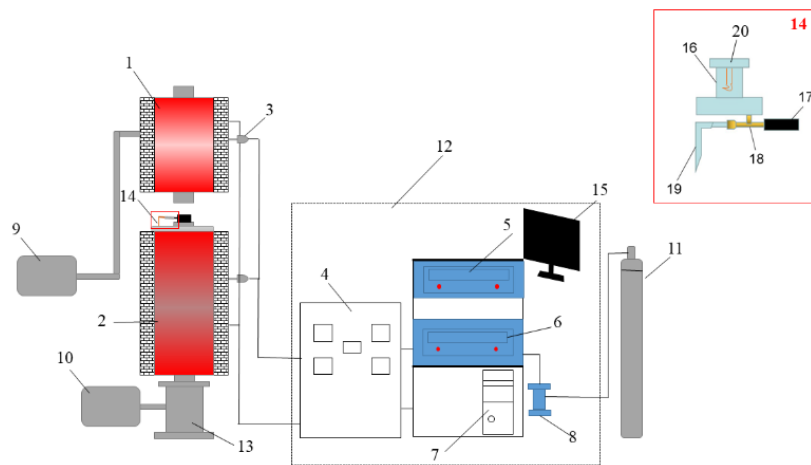


**Figure 2.** Experimental simulation device for BF coal injection. 1. Hot blast stove, 2. Pulverized coal combustion furnace, 3. Thermocouple, 4. Current and voltage display meter, 5. Hot blast stove console, 6. Pulverized coal combustion furnace console, 7. Computer, 8. Air flow meter, 9. Air compressor, 10. Drawing fan, 11. N<sub>2</sub> gas, 12. Data acquisition and control system, 13. UPC collecting tank, 14. Coal injection lance, 15. Computer monitor, 16. Coal bunker, 17. Sealed casing ring, 18. Copper injection pipe, 19. Gas nozzle and 20. Pulverized coal agitator.

### 2.2.2. Specific Surface Area

The specific surface area of the pulverized coal was characterized by a JW-BK112 specific surface area and pore size analyzer. The experiment followed the Chinese standard (GB/T19587-2004).

### 2.2.3. Microscopic Characterization

The micro-morphology of the two kinds of pulverized coal and UPC was characterized using a high-resolution field-emission scanning electron microscope (Nova400-Nano) at 1000× and 2000×.

### 2.2.4. Gasification Reaction

Gasification experiments were conducted using an HCT-3 thermal analyzer. Approximately 10-mg samples were placed in an alumina crucible (Φ6.5 mm × 1.5 mm) with 100 mL/min of carbon dioxide. The UPC obtained by the pulverized coal combustion test was heated from ambient temperature to 1250 °C at heating rates of 5 °C/min, 10 °C/min, 15 °C/min, and 20 °C/min.

The computer automatically collects the mass loss of UPC during the heating process, and the TG and DTG of the sample can be calculated by the following equations:

$$TG = \left( 100 - \frac{m_t - m_1}{m_e - m_1} \right) \times 100\% \quad (1)$$

$$DTG = -\frac{1}{m_1} \cdot \frac{dm}{dt} \times 100\% \quad (2)$$

where  $m_1$  is the initial mass of the sample at time  $t_1$ , mg;  $m_t$  is the mass of the sample at time  $t$ , mg; and  $m_e$  is the residual mass of the sample at the end of the reaction, mg.

### 3. Results and Discussion

#### 3.1. Combustion Conversion Degree of Pulverized Coal

The combustion conversion degree was calculated according to the ash balance calculation method [19,20]:

$$R = \frac{A_1 - A_0}{A_1 \times \left(1 - \frac{A_0}{100}\right)} \times 100\% \quad (3)$$

where  $R$  is the pulverized coal combustion conversion degree;  $A_0$  is the ash content before pulverized coal combustion, %; and  $A_1$  is the ash content of UPC, %. The combustion conversion degree results are shown in Table 2.

**Table 2.** Combustion conversion degree of Shenhua and Qingding pulverized coal (%).

Sample	Ash Content of UPC	Combustion Conversion Degree
Shenhua	13.17	65.43
Qingding	21.08	47.74

As shown in Table 2, the combustion conversion degree of the Shenhua pulverized coal is much higher than that of the Qingding pulverized coal. This can be explained as follows. Firstly, the volatile matter content of the Shenhua pulverized coal is higher than that of Qingding pulverized coal. The higher the volatile content is, the higher the degree of combustion conversion. Also, it can be observed in Figure 3 that most particles of Shenhua pulverized coal are rough and have obvious protrusions, which increases the contact area between the pulverized coal and oxygen. Furthermore, the specific surface area of the Shenhua pulverized coal is larger than that of Qingding pulverized coal, as shown in Figure 4, which enhances the adsorption of oxygen. Therefore, the Shenhua pulverized coal has a higher degree of combustion conversion.

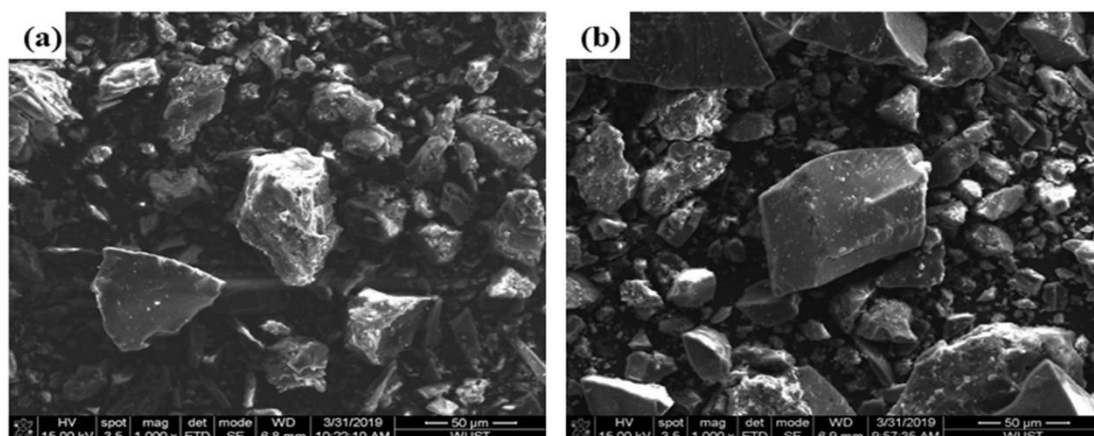


**Figure 3.** SEM image of Shenhua and Qingding pulverized coal: (a) Shenhua and (b) Qingding.

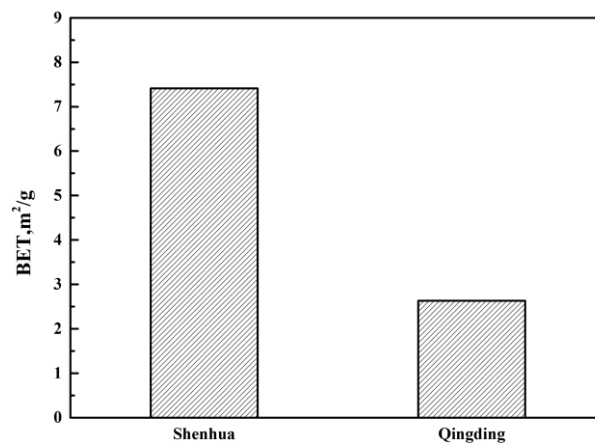


Figure 4. Brunauer-Emmett-Teller (BET) results for two kinds of pulverized coal.

### 3.2. Gasification Characteristics of UPC

The thermogravimetry (TG) and differential thermogravimetry (DTG) curves of the Shenhua UPC and Qingding UPC at heating rates of 5 °C/min, 10 °C/min, 15 °C/min and 20 °C/min are shown in Figures 5 and 6. Comparing the TG and DTG curves at the same heating rate, it can be seen that the Qingding UPC required a higher temperature to complete the gasification reaction. The maximum reaction rate temperature of the Shenhua UPC is lower and the reaction rate is higher. The gasification reaction of the Shenhua UPC is more intense. As the heating rate increases, the maximum reaction rate of both UPCs increases gradually. A higher heating rate enhances the gasification reaction of the UPCs.

To quantitatively analyze the difference between the gasification characteristics of the Shenhua UPC and Qingding UPC, the gasification result at the heating rate of 10 °C/min was selected, as shown in Figure 7. It can be observed that the reaction rate curves of the two kinds of UPC have similar characteristics with a single peak. The process of UPC gasification can be divided into three stages: preheating, rapid gasification reaction, and a termination stage. The second stage is the most intense during the gasification process, therefore, it will better reflect the gasification characteristics of the UPC. To quantitatively compare and analyze the gasification characteristics of the two UPCs, the gasification characteristic parameters were defined. The temperatures at conversion rates of 10% and 90% were defined as the gasification initial reaction temperature  $T_{10}$  and termination reaction temperature  $T_{90}$ , respectively. The temperature at the reaction rate peak was defined as  $T_m$ .

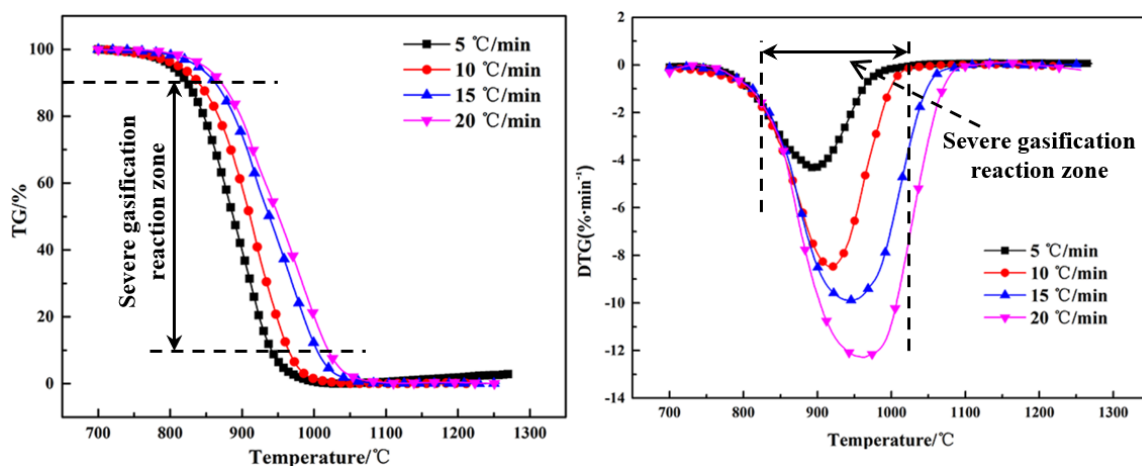


Figure 5. Thermogravimetry (TG) and differential thermogravimetry (DTG) curves of Shenhua UPC.

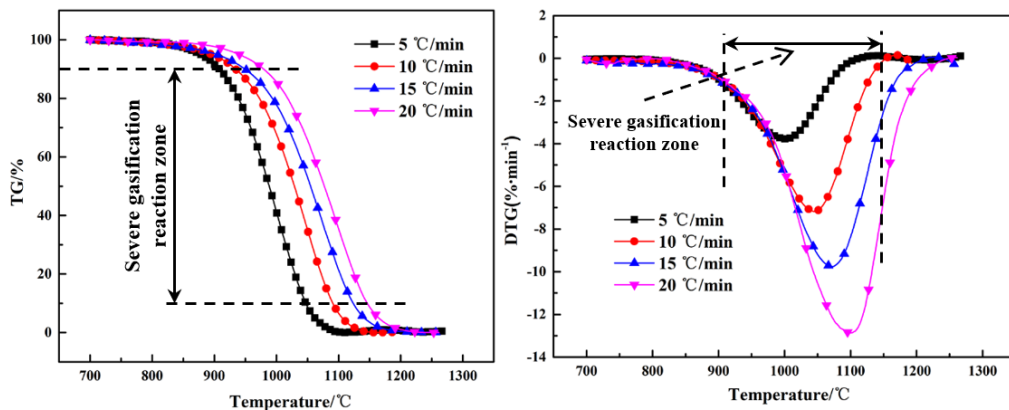


Figure 6. TG and DTG curves for Qingding UPC.

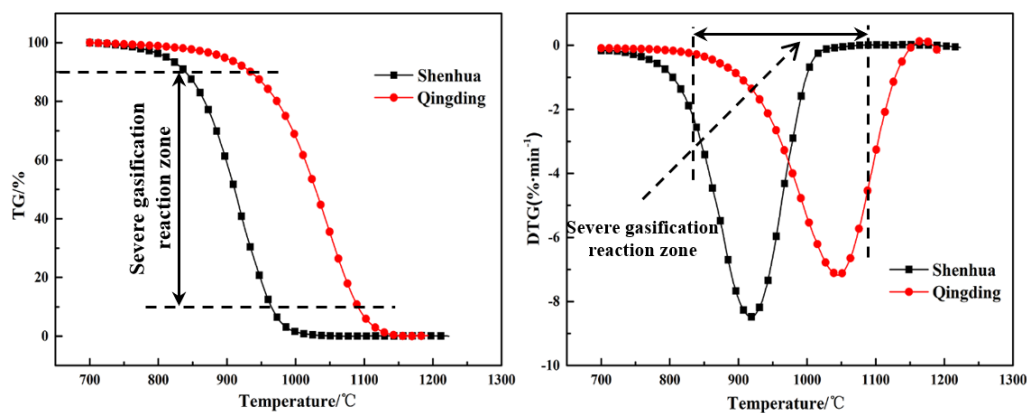


Figure 7. TG and DTG curves for Shenhua UPC and Qingding UPC at a heating rate of 10 °C/min.

The gasification characteristic parameters of the two UPCs are shown in Table 3. It can be seen from the table that  $T_{10}$ ,  $T_{90}$  and  $T_m$  of the Shenhua UPC are 839 °C, 964 °C and 919 °C, respectively, whereas  $T_{10}$ ,  $T_{90}$  and  $T_m$  of the Qingding UPC are 934 °C, 1090 °C and 1047 °C, respectively. The results show that  $T_{10}$ ,  $T_{90}$  and  $T_m$  of the Shenhua UPC are lower than those of the Qingding UPC, indicating that the gasification reaction of the Shenhua UPC begins at a lower temperature and the Qingding UPC needs higher temperatures to complete gasification.

Table 3. Characteristic temperatures of the gasification reaction of the different UPCs at 10 °C/min heating rate.

Sample	$T_{10}$ , °C	$T_m$ , °C	$T_{90}$ , °C
Shenhua	839	919	964
Qingding	934	1047	1090

### 3.3. Effect of the Heating Rate on the Gasification Behaviour of the UPC

Figures 5 and 6 show the TG and DTG curves for the Shenhua UPC and Qingding UPC at different heating rates. The gasification characteristic temperatures are listed in Table 4. Figures 5 and 6 show that as the heating rate increases, the gasification reaction curve gradually moves into the high temperature zone. From Table 4, it can be seen that as the heating rate increased, the characteristic temperature  $T_{10}$  of the Shenhua UPC increased from 824 °C to 871 °C,  $T_m$  increased from 893 °C to 961 °C, and  $T_{90}$  increased from 941 °C to 1019 °C. The characteristic temperature  $T_{10}$  of the Qingding UPC increased from 908 °C to 979 °C,  $T_m$  increased from 998 °C to 1099 °C, and  $T_{90}$  increased from 1047 °C to 1146 °C. Thus,  $T_{10}$ ,  $T_{90}$  and  $T_m$  increased with an increasing heating rate. On the one

hand, this phenomenon occurs because as the heating rate increases, CO<sub>2</sub> consumes less UPC at the same temperature. On the other hand, the gasification reaction of UPC is composed of two steps: heat transfer from the outside to the inside and mass transfer from the inside to the surface of UPC. The greater the heating rate, the greater the temperature difference between the inside and outside, resulting in the lag of heat and mass transfer.

**Table 4.** Characteristic temperature of gasification reaction of UPC under different heating rates.

Sample	Heating Rate (°C/min)	$T_{10}$ , °C	$T_m$ , °C	$T_{90}$ , °C
Shenhua UPC	5	824	893	941
	10	839	919	964
	15	863	945	1004
	20	871	961	1019
Qingding UPC	5	908	998	1047
	10	934	1047	1090
	15	949	1072	1123
	20	979	1099	1146

#### 3.4. Relationship between Structural Characteristics and Gasification Reaction of UPC

To further study the reasons for the different gasification reaction performance of the two UPCs, the microstructure of the UPC was characterized by SEM, as shown in Figure 8. Most of the Shenhua UPC particles have irregular protrusions and large open pores, which indicates that the combustion of Shenhua pulverized coal is very effective during the combustion experiment. Most of the surface of the Qingding UPC is relatively flat with no obvious protrusions. The open pores are smaller than those in the Shenhua UPC. Therefore, the Shenhua UPC has a larger contact area with CO<sub>2</sub>, and the gasification reaction is easier to develop than that in the Qingding UPC.

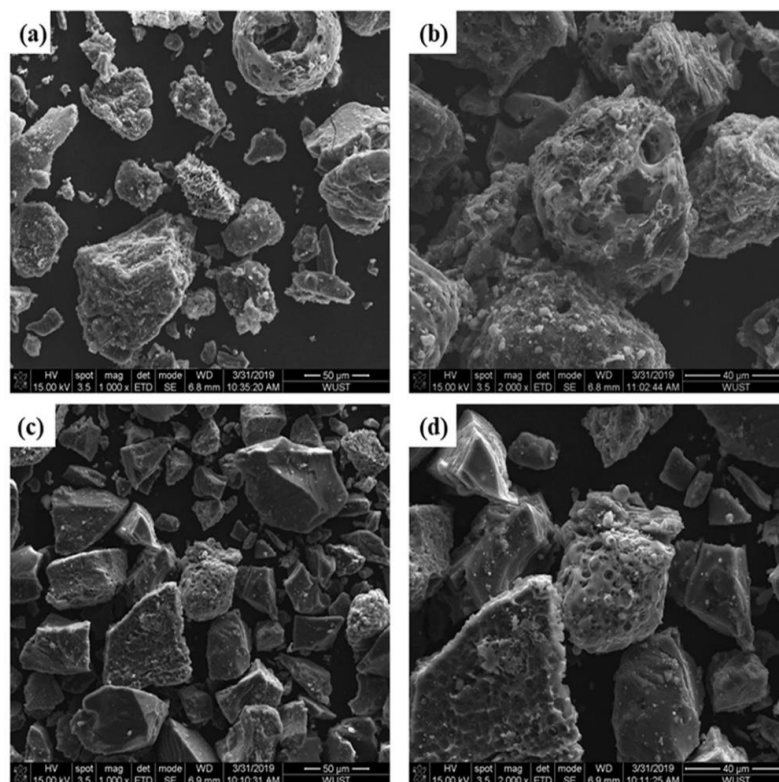


**Figure 8.** SEM image of (a,b) Shenhua UPC and (c,d) Qingding UPC.

### 3.5. Kinetics of UPC Gasification

During the entire UPC gasification process, the mass loss rate is a function of the reaction time and reaction temperature, and the functional relationship is expressed as:

$$\frac{dx}{dt} = k(T)f(x) \quad (4)$$

where  $\frac{dx}{dt}$  is the mass loss rate,  $s^{-1}$ ;  $k(T)$  is the rate constant, which is a function of temperature;  $f(x)$  is the differential form of the reaction mechanism function;  $t$  is the reaction time,  $s$ ; and  $x$  is the reaction conversion.

The rate constant  $k(T)$  is calculated by the Arrhenius equation:

$$k = A \exp\left(-\frac{E}{RT}\right) \quad (5)$$

where  $A$  is the pre-exponential factor;  $E$  is the activation energy,  $\text{kJ/mol}$ ; and  $R$  is the standard molar gas constant,  $\text{kJ mol}^{-1} \text{K}^{-1}$ .

During the non-isothermal heating process, the heating rate  $\beta$  is constant:

$$\beta = \frac{dT}{dt} \quad (6)$$

The following formula can be obtained from Equations (5) and (6):

$$\frac{dx}{dT} = \frac{A}{\beta} \exp\left(-\frac{E}{RT}\right) f(x) \quad (7)$$

Equation (7) can be integrated to give:

$$G(x) = \int_0^x \frac{dx}{f(x)} = \frac{A}{\beta} \int_0^T \exp\left(-\frac{E}{RT}\right) dT \quad (8)$$

Equations (9) and (10) can be obtained by the approximate calculation:

$$\frac{A}{\beta} \int_0^T \exp\left(-\frac{E}{RT}\right) dT \cong \frac{ART^2}{\beta E} \left(1 - \frac{2RT}{E}\right) \exp\left(-\frac{E}{RT}\right) \quad (9)$$

$$1 - \frac{2RT}{E} \cong 1 \quad (10)$$

The following formula can be obtained from Equations (9) and (10):

$$\ln\left[\frac{G(x)}{T^2}\right] = \ln\left(\frac{AR}{\beta E}\right) - \frac{E}{RT} \quad (11)$$

During an actual reaction,  $E$ ,  $A$  and  $\beta$  are constants; therefore,  $\ln(AR/\beta E)$  in Equation (11) is also a constant. A straight line can be obtained if the left-hand side of Equation (11) is plotted versus  $1/T$ . The slope of this line is  $-E/R$ , and the intercept is  $\ln(AR/\beta E)$ . The apparent activation energy  $E$  can be obtained by the slope, and the value of the pre-exponential factor  $A$  can be obtained by substituting  $E$  into the intercept. Through the coefficient of determination ( $R^2$ ), the most appropriate mechanism function of the UPC gasification reaction can be determined. Since the gasification reaction of the UPC is a typical gas-solid reaction, the general gas-solid reaction mechanism functions are used in this study, as shown in Table 5 [21–24].

Based on the gas-solid reaction mechanism functions, the gasification kinetics parameters of the two UPCs can be obtained. The gasification reaction is most intense during the second stage (rapid

gasification reaction stage) compared to the other two reaction stages as mentioned before, so the experimental data from this stage were used for model fitting and kinetic parameters calculation. When the heating rate is 5 °C/min, the kinetic parameters and the fitting results of the Shenhua UPC are shown in Table 6 and Figure 9, respectively. Table 6 shows that in the second reaction, the Shenhua UPC gasification belongs to the chemical reaction rate control model (F1), which has the highest R2 value. The results show that the gasification reaction of the Shenhua UPC at 5 °C/min is controlled by an interfacial chemical reaction.

**Table 5.** Mechanism functions of common gas-solid reaction models.

Mechanism	Code	Differential Form	Integral Form
Chemical reaction	N = 1 F1	$(1 - x)$	$-\ln(1 - x)$
	N = 2 F2	$(1 - x)^2$	$(1 - x)^{-1} - 1$
	N = 3 F3	$(1 - x)^3$	$[(1 - x)^{-2} - 1]/2$
Diffusion	The two-dimensional diffusion control D2	$[-\ln(1 - x)]^{-1}$	$x + (1 - x)\ln(1 - x)$
	The two-dimensional diffusion control (Jander function) D3	$1.5(1 - x)^{2/3}[1 - (1 - x)^{1/3}]$	$[1 - (1 - x)^{1/3}]^2$
	The three-dimensional diffusion control (Ginstling-Brounshten function) D4	$1.5[1 - (1 - x)^{1/3} - 1]^{-1}$	$(1 - 2x/3) - (1 - x)^{2/3}$
Shrinking core	Shrinking core R1	$2(1 - x)^{1/2}$	$1 - (1 - x)^{1/2}$
	Shrinking core R2	$3(1 - x)^{2/3}$	$1 - (1 - x)^{1/3}$
	Shrinking core (n = 2) R3	$\frac{1}{2}(1 - x)^{-1}$	$1 - (1 - x)^2$
Random nucleation and nuclei growth	Two-dimensional A2	$2(1 - x)[- \ln(1 - x)]^{1/2}$	$[- \ln(1 - x)]^{1/2}$
	Three-dimensional A3	$3(1 - x)[- \ln(1 - x)]^{2/3}$	$[- \ln(1 - x)]^{1/3}$

**Table 6.** Kinetic parameters of different mechanism functions of the Shenhua UPC in the second stage at 5 °C/min.

Code	Stage 2		
	E/(kJ/mol)	A/s <sup>-1</sup>	R <sup>2</sup>
F1	269.89	$1.12 \times 10^{11}$	0.9972
F2	380.22	$2.40 \times 10^{16}$	0.9933
F3	$3.95 \times 10^{-4}$	$2.83 \times 10^{-1}$	0.9873
D2	442.50	$2.03 \times 10^{18}$	0.9805
D3	498.68	$2.26 \times 10^{20}$	0.9915
D4	461.01	$3.50 \times 10^{18}$	0.9849
A2	125.35	$1.99 \times 10^4$	0.9966
A3	77.17	$8.92 \times 10$	0.9959
R1	$2.07 \times 10^{-4}$	$1.24 \times 10^{-1}$	0.9791
R2	$2.22 \times 10^{-4}$	$1.34 \times 10^{-1}$	0.9844
R3	$1.25 \times 10^{-4}$	$7.52 \times 10^{-2}$	0.9074

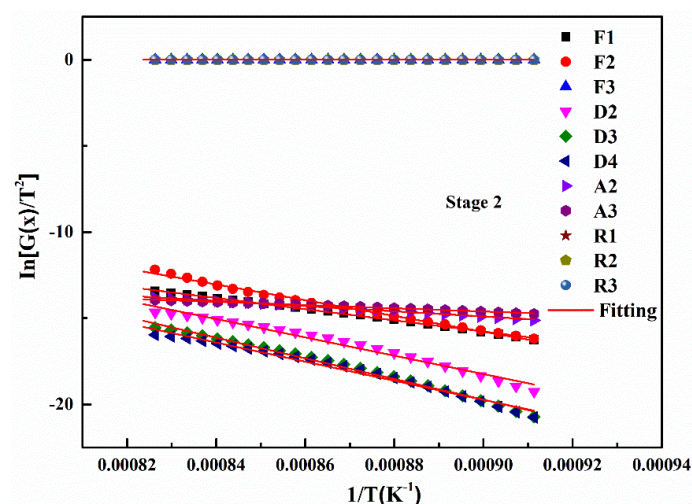


**Figure 9.** Linear fitting of the mechanism function for the second stage of the Shenhua UPC gasification reaction at 5 °C/min.

By using the abovementioned analysis method, the optimum mechanism function of the gasification reaction of the two UPCs at different heating rates can be confirmed, as shown in Figure 10. The kinetic parameters are shown in Table 7. According to the fitting results, it can be concluded that the gasification reactions for the two UPCs at different heating rates show the same reaction mechanism: a chemical reaction rate control of  $N = 1$  (F1). In Table 7 it can be seen that with the increase in heating rate, the apparent activation energy of Shenhua UPC decreased from 269.89 KJ/mol to 223.41 KJ/mol, and that of Qingding UPC decreased from 266.70 KJ/mol to 251.54 KJ/mol. When the heating rates are 5 °C/min, 10 °C/min and 15 °C/min, the apparent activation energies of the two UPCs are similar. However, the pre-exponential factor  $A$  of the Shenhua UPC is larger than that of the Qingding UPC. The results show that the molecular collision frequency of the Shenhua UPC is faster, so its reaction rate is higher. When the heating rate is 20 °C/min, the apparent activation energy of the Shenhua UPC is less than that of the Qingding UPC, indicating that the energy required for the gasification reaction of the Shenhua UPC is smaller. In summary, the Shenhua UPC gasification reaction occurs more easily than that of the Qingding UPC. In order to further verify consistency between the hypothesis of Equation (10) and the fitting results, the following calculations are carried out. As shown in Table 8. It can be seen that the assumption is appropriate in this study.

**Table 7.** Optimum mechanism function kinetic parameters for the second stage of the UPC gasification reaction at different heating rates.

Sample	Heating Rate	Stage/°C	Reaction Mechanism	E/(kJ/mol)	A/s <sup>-1</sup>	R <sup>2</sup>
Shenhua UPC	5 °C/min	2	F1	269.89	$1.12 \times 10^{11}$	0.9972
	10 °C/min	2	F1	265.16	$7.73 \times 10^{10}$	0.9995
	15 °C/min	2	F1	233.74	$2.26 \times 10^9$	0.9941
	20 °C/min	2	F1	223.41	$8.16 \times 10^8$	0.9922
Qingding UPC	5 °C/min	2	F1	266.70	$7.63 \times 10^9$	0.9998
	10 °C/min	2	F1	252.01	$1.63 \times 10^9$	0.9993
	15 °C/min	2	F1	235.43	$3.10 \times 10^8$	0.9989
	20 °C/min	2	F1	251.54	$1.43 \times 10^9$	0.9998

Table 8. Verification results of Equation (10).

Shenhua UPC	5 °C/min			10 °C/min		
	T(K)	R J/(mol*K)	E(kJ/mol)	T(K)	R J/(mol*K)	E(kJ/mol)
	1155.5	8.314	269.89	1174.5	8.314	265.16
	$1 - \frac{2RT}{E} = 0.93$			$1 - \frac{2RT}{E} = 0.93$		

It can be seen that the assumption is appropriate in this study.

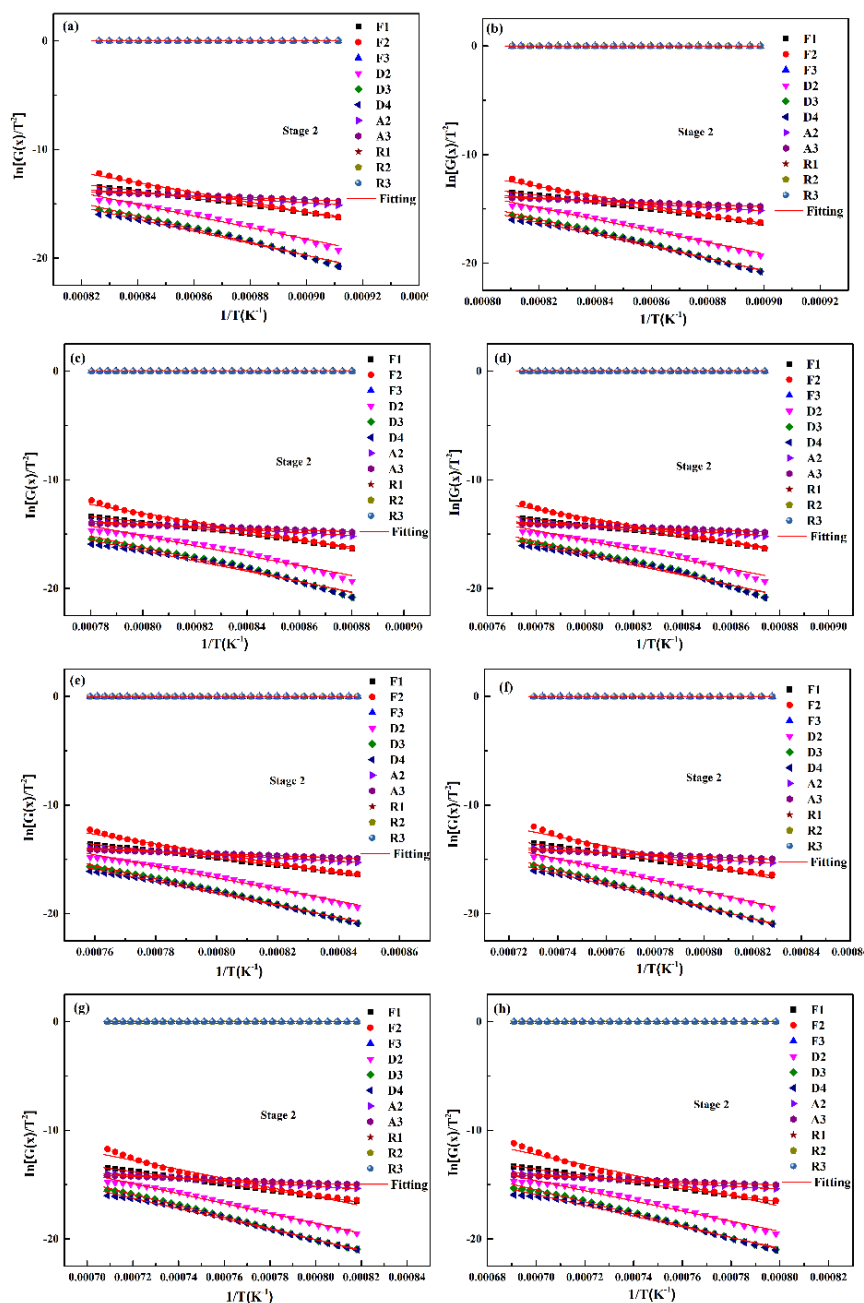


**Figure 10.** Linear fitting of the mechanism function for the second stage of the two UPCs at 5 °C/min, 10 °C/min, 15 °C/min and 20 °C/min: (a) Shenhua UPC at 5 °C/min, (b) Shenhua UPC at 10 °C/min, (c) Shenhua UPC at 15 °C/min, (d) Shenhua UPC at 20 °C/min, (e) Qingding UPC at 5 °C/min, (f) Qingding UPC at 10 °C/min, (g) Qingding UPC at 15 °C/min, and (h) Qingding UPC at 20 °C/min.

#### 4. Conclusions

In this paper, by studying the CO<sub>2</sub> gasification behavior and kinetics of two kinds of UPC at four different heating rates we were able to draw the following conclusions.

(1) Under the same conditions, the combustion conversion degree of Shenhua pulverized coal is larger than that of Qingding pulverized coal. A high volatile content, rough surface structure and high specific surface area are the reasons for the higher degree of combustion conversion of Shenhua pulverized coal than that of the Qingding pulverized coal.

(2) The gasification reaction occurs more easily for the Shenhua UPC than for the Qingding UPC, and the gasification reaction rate is much higher. The Qingding UPC requires a higher temperature to complete the gasification reaction. The Shenhua UPC has a lower  $T_m$  and a higher reaction rate than that of the Qingding UPC and the gasification reaction of the Shenhua UPC is more intense. The porous structure of the Shenhua UPC provides better kinetic conditions for its gasification reaction.

(3) The gasification reaction curves of the Shenhua and Qingding UPC gradually moved to a high temperature zone with an increasing heating rate. The maximum reaction rate of the UPCs gradually increased with an increasing heating rate.

(4) Under non-isothermal heating conditions, the optimum model for the two UPC gasification reactions is the chemical reaction model. The apparent activation energies of the Shenhua UPC and Qingding UPC are 269.89–223.41 KJ/mol and 266.70–251.54 KJ/mol, respectively.

**Author Contributions:** R.Z., W.W., and R.X. conceived and designed the experiments; R.Z. and H.W. performed the experiments; R.Z. and R.X. analyzed the data and wrote the original manuscript; J.S., H.Z. and R.X. reviewed and corrected the paper.

**Funding:** This research was funded by the National Natural Science Foundation of China grant number U1760101, 51704216, 51974212, 51474164.

**Acknowledgments:** The authors acknowledge financial support from the National Natural Science Foundation of China (U1760101, 51704216, 51974212, 51474164).

**Conflicts of Interest:** The authors declare no conflicts of interest.

#### References

1. Wang, H.T.; Zhao, W.; Chu, M.S.; Liu, Z.G.; Tang, J.; Ying, Z.W. Effects of coal and iron ore blending on metallurgical properties of iron coke hot briquette. *Powder Technol.* **2018**, *328*, 318–328. [[CrossRef](#)]
2. Wang, C.; Ryman, C.; Dahl, J. Potential CO<sub>2</sub> emission reduction for BF–BOF steelmaking based on optimised use of ferrous burden materials. *Int. J. Greenh. Gas Control* **2009**, *3*, 29–38. [[CrossRef](#)]
3. De Assis, C.F.C.; Tenório, J.A.S.; Assis, P.S.; Nath, N.K. Experimental Simulation and Analysis of Agricultural Waste Injection as an Alternative Fuel for Blast Furnace. *Energy Fuels* **2014**, *28*, 7268–7273. [[CrossRef](#)]
4. Assis, P.S.; Vieira, C.B.; Sobrinho, P.J.N. New Developments for Powder Coal Injection into the Blast Furnaces. *Steel Res. Int.* **2004**, *75*, 235–239. [[CrossRef](#)]
5. Halim, K.S.A.; Andronov, V.N.; Nasr, M.I. Blast furnace operation with natural gas injection and minimum theoretical flame temperature. *Ironmak. Steelmak.* **2009**, *36*, 12–18. [[CrossRef](#)]
6. Xu, R.S.; Dai, B.W.; Wang, W.; Schenk, J.; Xue, Z.L. Effect of iron ore type on the thermal behaviour and kinetics of coal-iron ore briquettes during coking. *Fuel Process. Technol.* **2018**, *173*, 11–20. [[CrossRef](#)]
7. Xu, R.S.; Zheng, H.; Wang, W.; Johannes, S.; Xue, Z.L. Influence of iron minerals on the volume, strength, and CO<sub>2</sub> gasification of ferro-coke. *Energy Fuels* **2018**, *32*, 12118–12127. [[CrossRef](#)]
8. Birk, W.; Marklund, O.; Medvedev, A. Video monitoring of pulverized coal injection in the blast furnace. *IEEE Trans. Ind. Appl.* **2002**, *38*, 571–576. [[CrossRef](#)]
9. Kazuyoshi, Y.; Hiromitsu, U.; Kenji, T. Maximum Injection Rate of Pulverized Coal into Blast Furnace through Tuyeres with Consideration of Unburnt Char. *ISIJ Int.* **1992**, *32*, 716–724. [[CrossRef](#)]
10. Mathieson, J.G.; Truelove, J.S.; Rogers, H. Toward an understanding of coal combustion in blast furnace tuyere injection. *Fuel* **2005**, *84*, 1229–1237. [[CrossRef](#)]

11. Xiang, D.W.; Shen, F.M.; Yang, J.L.; Jiang, X.; Zheng, H.Y.; Gao, Q.J.; Li, J.X. Combustion characteristics of unburned pulverized coal and its reaction kinetics with CO<sub>2</sub>. *Int. J. Miner. Metall. Mater.* **2019**, *26*, 811–821. [[CrossRef](#)]
12. Yu, Y.W.; Bai, C.G.; Liang, D.; Wang, F. Numerical simulation characteristics of unburned pulverised coal in blast furnace. *Ironmak. Steelmak.* **2009**, *36*, 279–285. [[CrossRef](#)]
13. Diao, R.S.; Hu, B.S. Behavior of unburned particle in blast furnace pulverized coal injection. *Iron Steel Vanadium Titan.* **2003**, *24*, 18–21. [[CrossRef](#)]
14. Yu, Q.Y. Experiment Research on BF Unburned Pulverized Coal and Carbon Consumption. *Baosteel Technol.* **2004**, 29–32. [[CrossRef](#)]
15. Yu, Q.Y.; Cao, J.; Shen, F.M. Experiment research on effect of unburned pulverized coal on coke reactivity in blast furnace. *Baosteel Technol.* **2006**, 31–34. [[CrossRef](#)]
16. Takashi, S. Experimental and numerical analysis on the movement and the accumulation of powder in the deadman and the dripping zone of blast furnace. *Tetsuto-Hagane* **1996**, *82*, 29–34. [[CrossRef](#)]
17. Diao, R.S.; Hu, B.S. Influence of unburned PCI on the blast furnace slag viscosity in Panzhihua Steel Co. *Iron Steel* **2004**, *39*, 14–16. [[CrossRef](#)]
18. Iwanaga, Y. Gasification rate analysis of unburnt pulverized coal in blast furnace. *ISIJ Int.* **1991**, *31*, 500–504. [[CrossRef](#)]
19. Du, S.W.; Chen, W.H.; Lucas, J.A. Pulverized coal burnout in blast furnace simulated by a drop tube furnace. *Energy* **2010**, *35*, 576–581. [[CrossRef](#)]
20. Chen, W.H.; Du, S.W.; Tsai, C.H.; Wang, Z.Y. Torrefied biomasses in a drop tube furnace to evaluate their utility in blast furnaces. *Bioresour. Technol.* **2012**, *111*, 433–438. [[CrossRef](#)]
21. Zheng, H.; Wang, W.; Xu, R.S.; Zan, R.A.; Schenk, J.; Xue, Z.L. Effect of the particle size of iron ore on the pyrolysis kinetic behaviour of coal-iron ore briquettes. *Energies* **2018**, *11*, 2595. [[CrossRef](#)]
22. Zhang, S.F.; Zhu, F.; Bai, C.G.; Wen, L.Y.; Peng, H.J. High temperature pyrolysis behaviour and kinetics of lump coal in COREX melter gasifier. *Ironmak. Steelmak.* **2013**, *41*, 219–228. [[CrossRef](#)]
23. Li, P.; Yu, Q.; Xie, H.; Qin, Q.; Wang, K. CO<sub>2</sub> Gasification rate analysis of datong coal using slag granules as heat carrier for heat recovery from blast furnace slag by using a chemical reaction. *Energy Fuels* **2013**, *27*, 4810–4817. [[CrossRef](#)]
24. Vlaev, L.T.; Markovska, I.G.; Lyubchev, L.A. Non-isothermal kinetics of pyrolysis of rice husk. *Thermochim. Acta* **2003**, *406*, 1–7. [[CrossRef](#)]



© 2019 by the authors. Licensee MDPI, Basel, Switzerland. This article is an open access article distributed under the terms and conditions of the Creative Commons Attribution (CC BY) license (<http://creativecommons.org/licenses/by/4.0/>).